The FASEB Journal article fj.201600643R. Published online September 23, 2016.

Lipid raft–associated stomatin enhances cell fusion

Jui-Hao Lee,[*,†,‡] Chia-Fen Hsieh,[†] Hong-Wen Liu,[†,§] Chin-Yau Chen,[†,¶] Shao-Chin Wu,[‖] Tung-Wei Chen,[‖] Chih-Sin Hsu,[†] Yu-Hsiu Liao,[‖] Chih-Yung Yang,[**] Jia-Fwu Shyu,[††] Wolfgang B. Fischer,[‖] and Chi-Hung Lin[*,†,‖,1]

[*]Taiwan International Graduate Program in Molecular Medicine, National Yang-Ming University and Academia Sinica, Taipei, Taiwan; [†]Institute of Microbiology and Immunology, [‡]Institute of Biochemistry and Molecular Biology, [§]Chong Hin Loon Memorial Cancer and Biotherapy Research Center, and [‖]Institute of Biophotonics, National Yang-Ming University, Taipei, Taiwan; [¶]Department of Surgery, I-Lan, Taiwan; [**]Department of Education and Research, Taipei City Hospital, Taipei, Taiwan; and [††]Department of Biology and Anatomy, National Defense Medical Center, Taipei, Taiwan

ABSTRACT: Membrane fusions that occur during vesicle transport, virus infection, and tissue development, involve receptors that mediate membrane contact and initiate fusion and effectors that execute membrane reorganization and fusion pore formation. Some of these fusogenic receptors/effectors are preferentially recruited to lipid raft membrane microdomains. Therefore, major constituents of lipid rafts, such as stomatin, may be involved in the regulation of cell–cell fusion. Stomatin produced in cells can be released to the extracellular environment, either through protein refolding to pass across lipid bilayer or through exosome trafficking. We report that cells expressing more stomatin or exposed to exogenous stomatin are more prone to undergoing cell fusion. During osteoclastogenesis, depletion of stomatin inhibited cell fusion but had little effect on tartrate-resistant acid phosphatase production. Moreover, in stomatin transgenic mice, increased cell fusion leading to enhanced bone resorption and subsequent osteoporosis were observed. With its unique molecular topology, stomatin forms molecular assembly within lipid rafts or on the appositional plasma membranes, and promotes membrane fusion by modulating fusogenic protein engagement.—Lee, J.-H., Hsieh, C.-F., Liu, H.-W., Chen, C.-Y., Wu, S.-C., Chen, T.-W., Hsu, C.-S., Liao, Y.-H., Yang, C.-Y., Shyu, J.-F., Fischer, W. B., Lin, C.-H. Lipid raft–associated stomatin enhances cell fusion. FASEB J. 31, 000–000 (2017). www.fasebj.org

KEY WORDS: exosome · membrane permeability · osteoclastogenesis

Cell fusion plays an important role in cell differentiation and development, injury repair, and various pathogenic processes (1–5). Similar to vesicular fusion, cell fusion involves several highly orchestrated steps (6–8), including establishment of membrane contact, formation of a fusion stalk, hemifusion, formation of fusion pores, and complete fusion. Receptor and effector protein complexes, such as soluble *N*-ethylmaleimide–sensitive factor-activating protein receptor (SNARE) assembly in vesicle transport, hemagglutinin in viral infection, the fusogen family of proteins (EFF-1 and AFF-1) in *Caenorhabditis elegans* development, and syncytin in placental morphogenesis, support the formation of hairpin structure and zippering mechanisms that are instrumental in membrane fusion (4, 7–11). In addition, there is increasing evidence that lipid rafts, together with adhesion proteins and actin rearrangement, are critical for the formation and expansion of fusion pores in the final step of membrane fusion (12–16).

Lipid rafts on cell membranes are microdomains with abundant cholesterol and sphingolipids. They have been demonstrated to play an important role in response to intracellular or extracellular triggering. Lipid rafts change in size and composition *via* clustering and partitioning (17–20). This dynamic provides a versatile platform for regulation of intermolecular interactions among receptors and effectors of opposing membranes during cell fusion. In osteoclastogenesis, disruption of lipid rafts can profoundly inhibit cell fusion in multinuclear osteoclast (OC) formation (14). Previous findings have implied that stomatin, a major component of lipid rafts (21), is enriched in the raft domain of the vesicular membrane, which delivers

ABBREVIATIONS: μ-CT, microcomputed tomography; 3D, 3-dimensional; BMDC, bone marrow–derived cell; BSA, bovine serum albumin; CCD, charge-coupled device; CHO, Chinese hamster ovary; CM, conditioned medium; DC-STAMP, dendritic cell–specific transmembrane protein; EGFP, enhanced GFP; FBS, fetal bovine serum; GFP, green fluorescent protein; GST, glutathione *S*-transferase; HEK, human embryonic kidney; HSP, heat shock protein; hSTOM, human stomatin; M-CSF, macrophage–colony stimulating factor; MNC, multinuclear cell; mOC, mononuclear OC; mStom, murine stomatin; OC, osteoclast; OCP, OC progenitor; RANKL, receptor activator of nuclear factor-κB ligand; RFP, red fluorescent protein; shRNA, short hairpin RNA; STOM-Tg, stomatin transgenic; TBS-T, Tris-buffered saline–0.1% Tween 20; TRAP, tartrate-resistant acid phosphatase; WT, wild-type

[1] Correspondence: Institute of Microbiology and Immunology, National Yang-Ming University, 155, Li-Nong St., Sec. 2, Taipei, Taiwan 112. E-mail: linch@ym.edu.tw

doi: 10.1096/fj.201600643R
This article includes supplemental data. Please visit *http://www.fasebj.org* to obtain this information.

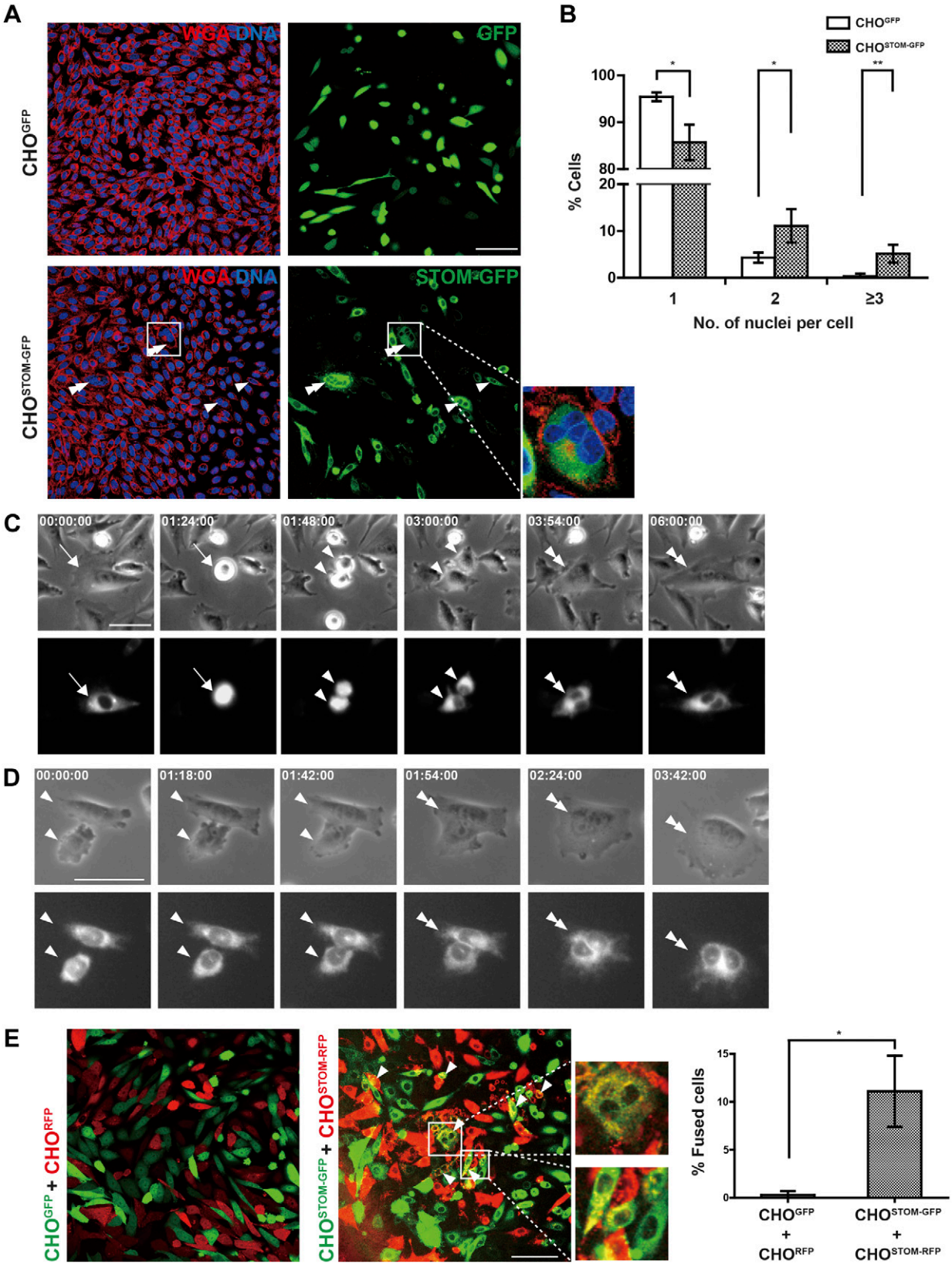

Figure 1. Stomatin induces MNC formation *via* refusion and cell fusion. *A*) CHO cells transfected with *STOM-GFP* ($CHO^{STOM\text{-}GFP}$) or control *GFP* gene (CHO^{GFP}) were cultured for 3 d and stained with wheat germ agglutinin (WGA, red) to reveal cell membrane and Hoechst 33342 to label DNA (blue). Representative images of MNCs found in $CHO^{STOM\text{-}GFP}$ cells show that they contained 2 (arrowheads) or more nuclei per cell (double arrowheads and inset). Scale bar, 75 μm. *B*) Quantification of MNCs in 3-d culture of CHO^{GFP} or $CHO^{STOM\text{-}GFP}$ cells as a function of nucleus number per cell ($n = 642$ and 888 total counted CHO^{GFP} and $CHO^{STOM\text{-}GFP}$ cells, respectively, in 3 independent experiments). *C*, *D*) Time-lapse recording (h/min/s) of live STOM-GFP-

(*continued on next page*)

intercellular signals and promotes membrane merging (22–24).

Stomatin is a small protein (31.5 kDa) named after human hemolytic anemia hereditary stomatocytosis, and it is also called overhydrated hereditary stomatocytosis (25, 26). The murine erythrocytes in stomatin gene–deleted mice are the same as in wild-type (WT) mice in red blood cell morphology and physiology (27). Because of its specialized structural features, including hydrophobic domain, palmitoylation, and oligomerization (28–31), stomatin can be targeted to the membrane to regulate receptors through intermolecular action. In addition, insertion of stomatin into the membrane can create an imbalance of protein and lipid interface that reorganizes the membrane structure (32), but the membrane topology is still uncertain (33). During cell–cell fusion, the formation of the fusion stalk necessitates membrane bending to enter into the stage of hemifusion, and the curvature is essential for fusion pore expansion (34). The membrane surface of stomatin-deficient erythrocytes is less curved than in normal erythrocytes (26, 35), which may suggest that stomatin modulates membrane bending, thereby affecting the curvature of the membrane.

We addressed whether and how stomatin affects cell fusion activity by using various cell lines and microscopic approaches. Expression of stomatin and exposure to extracellular stomatin (conditioned media or recombinant protein) can induce different types of cells to form multinuclear cells (MNCs) resulting from cell–cell fusion. Stomatin knockdown leads to obvious inhibition of receptor activator of nuclear factor-κB ligand (RANKL)–induced cell fusion in OC formation and increased expression of stomatin can enhance cell fusion in murine monocytes/macrophages and promote osteoporosis. We proposed that lipid raft–associated stomatin enhances intermolecular action by clustering fusogenic assemblies, thus potentiating cell fusion and releasing the membrane-bending stresses by supplying a platform for actin polymerization to generate forces.

MATERIALS AND METHODS

Cell culture

Chinese hamster ovary (CHO) K1 cells, purchased from Bioresource Collection and Research Center (no. 60006; Bioresource Collection and Research Center, Hsinchu, Taiwan), were maintained in F12 medium supplemented with 10% fetal bovine serum (FBS) and 1% L-glutamine (200 mM stock solution; HyClone, GE Healthcare Life Science, South Logan, UT, USA). RAW264.7 macrophage/monocyte (60001, Bioresource Collection and Research Center), and human embryonic kidney (HEK) 293T cells were cultured in DMEM supplemented with 10% FBS.

Plasmid construction and transfection

For transfection plasmid construction, the coding region from cDNA clone MGC: 9177 (BC010703), containing complete human stomatin cDNA sequence human (h)*STOM*, was purchased from YMGC (National Yang-Ming University Genome Research Center, Taipei, Taiwan) and cloned into pLPS-3′EGFP (Clontech, Mountain View, CA, USA) or pLPS-3′RFP (Clontech) expression vectors. CHO-K1 (5.0×10^5) or HEK-293T (1.0×10^6) cells were seeded in 35 mm dishes. After overnight incubation, the cells were transfected with either plasmid DNA, with T-Pro NTR-II transfection reagent (T-Pro Biotechnology, New Taipei City, Taiwan) according to the manufacturer's instructions. At 16 h after transfection, CHO^{GFP} and $CHO^{STOM\text{-}GFP}$, CHO^{RFP} and $CHO^{STOM\text{-}RFP}$, or $293T^{GFP}$ and $293T^{STOM\text{-}GFP}$ cells were subcultured.

Lentivirus production and transduction

Vector pLKO-AS2.puro was obtained from National RNAi Core Facility Platform (Academia Sinica, Taipei, Taiwan), and *EGFP*, *RFP*, *STOM-EGFP*, and *STOM-RFP* were amplified from expression plasmids and cloned into the lentiviral vector. In addition, the lentiviral plasmid construct of pLKO-AS2.puro-*STOM* contains h*STOM* sequence. Gene knockdown constructs, shRNA-*Luc*-KD or shRNA-*STOM*-KD vectors, were acquired from the National RNAi Core Facility Platform; the clone numbers of shRNA-STOM-KD1 and -KD2 were TRCN0000112911 and TRCN0000112912, respectively. To generate lentiviruses, HEK-293T cells were plated in 35 mm culture dishes and transfected with lentivirus packaging plasmids: pMD.G and pCMVΔR8.91 (National RNAi Core Facility Platform) and pLKO-AS2.puro expression or short hairpin (sh) RNA vectors were mixed with T-Pro NTR-II transfection reagent after overnight incubation. At 16 h after transfection, medium containing transfection reagent was replaced with 40% FBS DMEM. Medium containing lentiviruses was harvested at 40 and 64 h after transfection and used to transduce CHO-K1 (CHO^{STOM}, CHO^{GFP}, $CHO^{STOM\text{-}GFP}$, CHO^{RFP}, and $CHO^{STOM\text{-}RFP}$) and RAW264.7 (RAW^{RFP}, and $RAW^{STOM\text{-}RFP}$) cells, followed by puromycin selection for 3 d. All experiments were performed in a biosafety level 2 laboratory.

Protein expression and purification

h*STOM* was cloned into the pBiEx-2 vector (EMD–Millipore, Billerica, MA, USA) and expressed as N-terminal glutathione *S*-transferase (GST)–tagged fusion proteins (GST-STOM) in BL21-CodonPlus (DE3)-RIPL–competent cells (Agilent Technologies, Santa Clara, CA, USA). The competent cells were grown in Luria-Bertani medium with 1 mM isopropyl β-D-1-thiogalactopyranoside induction for protein expression, followed by 3 h incubation at 30°C. After induction, cells were resuspended in ice-cold PBS,

or STOM-RFP-transfected CHO cells by phase-contrast and fluorescence microscopy. Scale bar, 50 μm. *C*) The $CHO^{STOM\text{-}RFP}$ cells entering mitosis at time 0 (arrow) were noted to stop at cytokinesis (from 01:48:00 to 03:00:00). As a result of cytokinesis failure, 2 putative daughter cells (arrowheads) refused and formed a cell containing 2 nuclei (double arrowhead). *D*) Two independent $CHO^{STOM\text{-}GFP}$ cells (arrowheads) came into contact, interacted, and fused into a cell with 2 nuclei (double arrowhead). *E*) CHO cells separately transduced by lentiviral vector to express STOM-GFP ($CHO^{STOM\text{-}GFP}$) or STOM-RFP ($CHO^{STOM\text{-}RFP}$) were cocultured for 3 d. Cells having both green and red fluorescence (appear yellow), indicative of cell fusion, were identified by confocal microscopy (arrowheads) and quantified as percentage of fused cells ($n = 2445$ total counted cells). Cocultured CHO cells transduced with GFP or RFP were used as controls ($n = 2808$ total counted cells). Scale bar, 75 μm. All data are means ± SD from 3 independent experiments. $^*P < 0.05$, $^{**}P < 0.01$, by paired Student's *t* test.

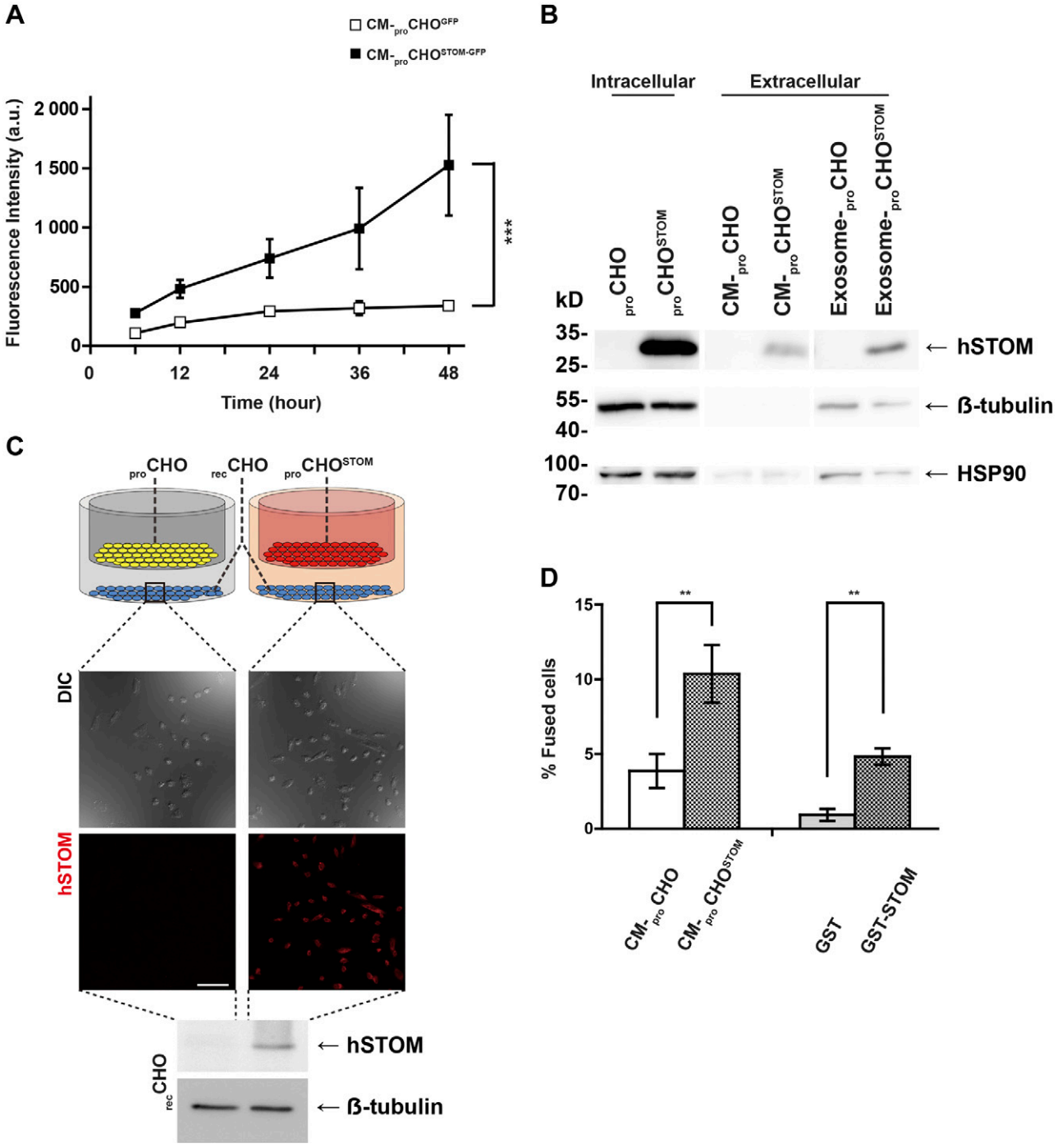

Figure 2. Extracellular stomatin affects other cells. *A*) CM-$_{pro}$CHO$^{STOM\text{-}GFP}$ and CM-$_{pro}$CHO^{GFP} [CM from CHO cells transfected with STOM-GFP ($_{pro}$CHO$^{STOM\text{-}GFP}$) or control GFP ($_{pro}$CHO^{GFP}) gene] were subjected to fluorophotometry analysis. Note the progressive increase of fluorescence over time in CM-$_{pro}$CHO$^{STOM\text{-}GFP}$ compared to CM-$_{pro}$CHO^{GFP} cells, indicating detection of released stomatin by $_{pro}$CHO$^{STOM\text{-}GFP}$ cells. Data are means ± SD from 5 independent experiments (each with 3 technical replicates). ***$P < 0.001$, by 2-way ANOVA. *B*) Samples of CHO cells transduced with stomatin ($_{pro}$CHO^{STOM}) or control vector ($_{pro}$CHO), TCA-precipitated proteins (CM of CM-$_{pro}$CHO^{STOM} or CM-$_{pro}$CHO, respectively), and collected exosomes from 3 d culture media were subjected to Western blot analysis. hSTOM proteins were present not only in $_{pro}$CHO^{STOM} cells, but also in their extracellular culture media. β-Tubulin was not detected in CM. HSP90 protein was an exosomal marker ($n = 5$ independent experiments). *C*) $_{pro}$CHO or $_{pro}$CHO^{STOM} cells were seeded in the upper chamber of a cell migration assay system (0.4 μm–sized pores) and protein receiver $_{rec}$CHO cells were plated in the lower chamber. After 3 d, $_{rec}$CHO cells were subjected to immunofluorescence staining and Western blot to reveal uptake of stomatin by $_{rec}$CHO. A representative example is shown ($n = 5$ independent experiments.) Scale bar, 50 μm. *D*) CM of CM-$_{pro}$CHO^{STOM} or CM-$_{pro}$CHO cells, bacteria-expressed recombinant protein GST, or stomatin conjugated with GST (GST-STOM) was added to mixed cultured cells separately labeled with either CellTracker Red or CellTracker Green. After 3 d, cells containing both CellTracker dyes (indicative of fused cells) were identified and quantified. [*N* (total counted cells) = 1147, 1405, 1950, and 1860 for CM-$_{pro}$CHO, CM-$_{pro}$CHO^{STOM}, GST, and GST-STOM treated cells, respectively]. Data are means ± SD from 4 (CM) and 3 (recombinant protein) independent experiments, respectively. **$P < 0.01$, by paired Student's *t* test.

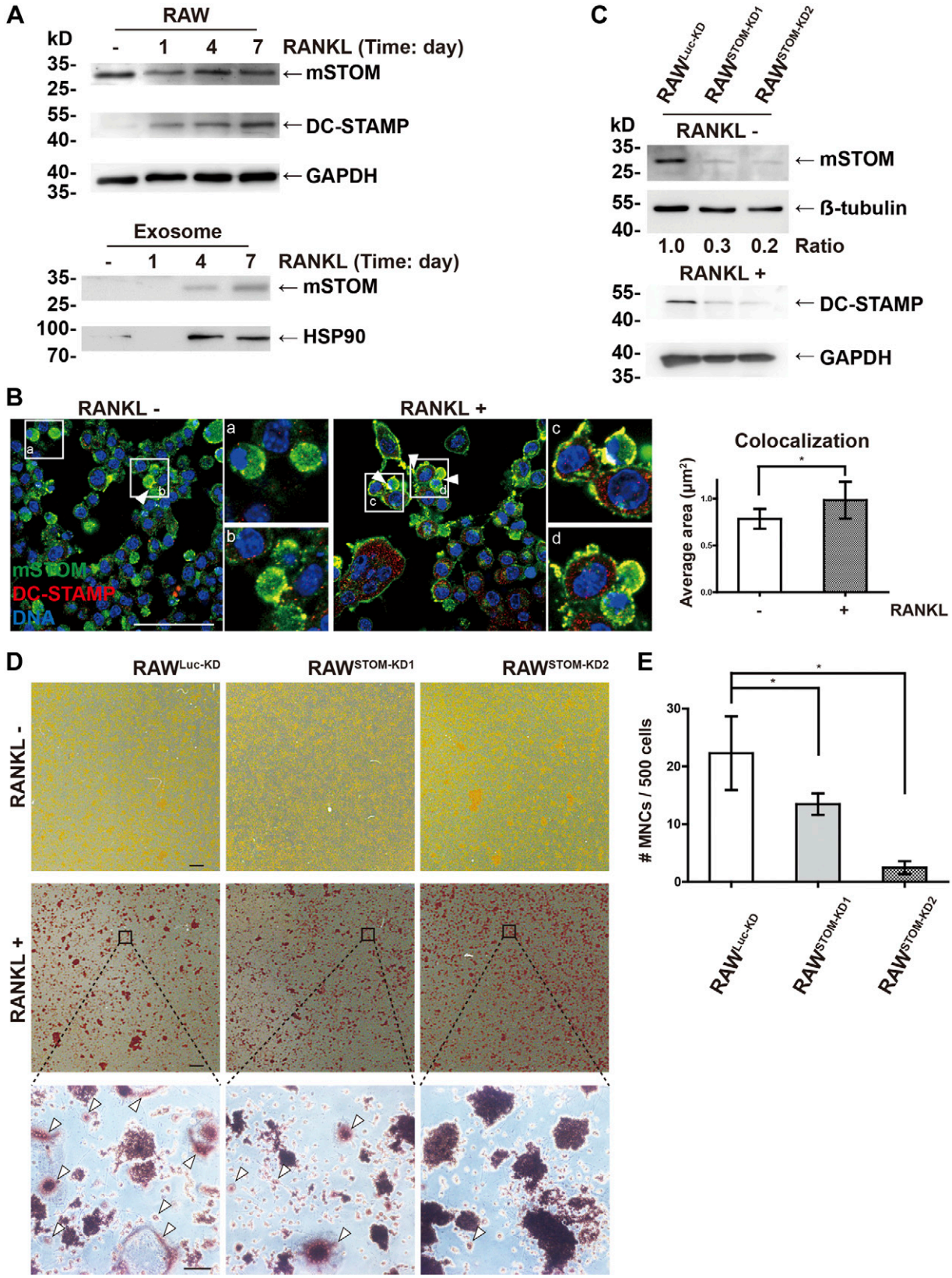

Figure 3. Stomatin is involved in osteoclastogenesis. *A*) Samples of RANKL-treated or untreated RAW cells, and exosomes from culture media were subjected to Western blot analysis. RANKL stimulation increased DC-STAMP expression in a time-dependent manner. mStom proteins were increased in both cell lysates and extracellular exosomes from d 1 to 7 during RANKL treatment. GAPDH was used as the loading control and HSP90 as an exosomal marker ($n = 5$ independent experiments). *B*) Localization of mStom (Cy5 conjugation; green) and DC-STAMP (tetramethylrhodamine conjugation; red) in RANKL-treated or untreated RAW cells was analyzed by immunofluorescence assay with DNA labeling (blue). RANKL-induced RAW cells displayed a

(*continued on next page*)

passed through a French press, and centrifuged at 15,000 *g* for 10 min at 4°C. The supernatant was purified with GSTrap FF columns with a GST buffer kit (GE Healthcare Life Science, Pittsburgh, PA, USA), according to the manufacturer's protocol. The proteins were concentrated by using Amicon Ultra-15 with Ultracel-30 membrane (EMD-Millipore). Cell fusion was examined with 100 μg/ml protein (0.5 μg/μl).

Cell multinucleation and fusion analysis

CHO-K1 cells transfected with pLPS-3′EGFP or pLPS-STOM-3′EGFP were observed from d 1 to 3 for MNCs under an inverted microscope (DM-IRBE; Leica, Wetzlar, Germany) with a cooled charge-coupled device camera (CCD; ORCA-ER; Hamamatsu, Hamamatsu City, Japan), with a ×20 0.40 NA or 40 0.60 N Plan objective lens (Leica) or a confocal microscope (SP5; Leica), with a ×40 1.25 NA, 63 1.40, or 100 1.40 HCX PL APO objective lens (Leica). Cell membranes and nuclei were labeled with the ImageiT Live plasma membrane and nuclear labeling kit (Thermo Fisher Scientific, Waltham, MA, USA) to distinguish MNCs from mononuclear cells. The number of MNCs and nuclei per cell was analyzed with MetaMorph Software (Molecular Devices, Sunnyvale, CA, USA). Cell fusion events in mixed cultures of transfected or lentiviral transduced CHO^{GFP} and CHO^{RFP} or $CHO^{STOM\text{-}GFP}$ and $CHO^{STOM\text{-}RFP}$, respectively, were recorded with a CCD camera (ORCA-ER; Hamamatsu) on an inverted (DM-IRBE; Leica) or confocal (SP5; Leica) microscope. To compare cell fusion between different animal species, HEK-293T cells transfected with pLPS-STOM-3′EGFP were cocultured with CHO-K1 cells transfected with pLPS-STOM-3′RFP, and HEK-293T/CHO-K1 cells transfected with GFP/RFP were used as the control. In addition, the number of fused cells was analyzed by flow cytometry (FACSCalibur; BD Biosciences, Franklin Lakes, NJ, USA).

Conditioned medium preparation and treatment

Conditioned medium (CM) from protein-expressing cells (producers) $_{pro}CHO^{GFP}$ (pLPS-3′EGFP) or $_{pro}CHO^{STOM\text{-}GFP}$ (pLPS-STOM-3′EGFP) cells was collected and passed through a 0.20 μm filter (EMD Millipore) to remove cell debris for analysis of extracellular protein stomatin-GFP on a fluorescence microplate reader with excitation 480 nm and emission 520 nm (Infinite200; Tecan, Männedorf, Switzerland). Three-day culture medium (F12 supplemented with 1% L-glutamine) from the lentiviral transduced clones $_{pro}CHO$ (pLKO-AS2.puro) or $_{pro}CHO^{STOM}$ (pLKO-AS2.puro-*STOM*) cells (producers) was collected, filtered (0.20 μm), and subjected to trichloroacetic acid (Sigma-Aldrich, St. Louis, MO, USA) precipitation, to concentrate the proteins for Western blot analysis. To reveal CM-induced MNCs, Transwell cell-migration assay plates (pore size, 0.4 μm; EMD–Millipore) were used to coculture receiver cells ($_{rec}CHO$) in the bottom chamber and seeding either $_{pro}CHO$ or $_{pro}CHO^{STOM}$ cells in the upper chamber for 3 d. To investigate cell fusion, the cells were labeled with CellTracker Green CMFDA or CellTracker Red CMTPX in a 10 μM working concentration (Thermo Fisher Scientific) with CM treatment. The total exosomes were purified with Total Exosome Isolation reagents (Thermo Fisher Scientific), according to the manufacturer's protocol.

Western blot analysis

Cells and exosomes were lysed with RIPA solution supplemented with protease inhibitor cocktail (EMD–Millipore). Proteins were separated on SDS-polyacrylamide gels and then transferred by SDS-PAGE onto PVDF membranes (EMD–Millipore). After they were blocked with 5% bovine serum albumin (BSA) in Tris-buffered saline–0.1% Tween 20 (TBS-T) at room temperature for 1 h, the membranes were incubated with anti-hSTOM (dilution: 1:500; M-14; Santa Cruz Biotechnology, Dallas, TX, USA), anti-mStom (dilution: 1:500; N-14; Santa Cruz Biotechnology), anti-dendritic cell–specific transmembrane protein (anti-DC-STAMP; dilution: 1:200; 1A2; EMD–Millipore), anti-heat shock protein (HSP)90α (dilution 1:3,000; EMD-17D7; EMD–Millipore), anti-GAPDH (dilution: 1:10,000; Sigma-Aldrich), or anti-tubulin (dilution: 1:10,000; Sigma-Aldrich) antibodies at 4°C overnight. The membranes were washed 3 times for 10 min each with TBS-T and then incubated with appropriate horseradish peroxidase–conjugated secondary antibodies (dilution: 1:5000; Santa Cruz Biotechnology) for 1 h at room temperature. Western blot signals were visualized with SuperSignal West Femto Maximum Sensitivity Substrate (Thermo Fisher Scientific) and imaged with ImageQuant LAS-4000 (GE Healthcare Life Science).

Immunofluorescence staining

Cells seeded on coverslips were fixed with 3.7% formaldehyde (Sigma-Aldrich) at room temperature for 15 min and then rinsed twice with PBS for 5 min. After fixation, the cells were permeabilized with 0.01% TX-100 for 5 min, washed 3 times with PBS for 5 min each, and blocked with 5% BSA blocking solution for 60 min. Permeabilized cells were probed with the appropriate dilution (1:200) of antibodies: anti-hSTOM (M-14), anti-mStom (N-14), and anti-DC-STAMP (1A2) in blocking solution overnight, in a humid chamber at 4°C. The cells were then washed 3 times in PBS for 10 min each and incubated with fluorophore-conjugated (dilution: 1:500; AlexaFluor-488, tetramethylrhodamine, or Cy5) secondary antibodies (Jackson ImmunoResearch, West Grove, PA, USA) in blocking solution for 1 h at room temperature. The cell samples were labeled with Hoechst 33342 to mark nuclei, mounted with anti-photobleaching medium, and observed by confocal microscopy (SP5; Leica). For analysis of colocalization of mStom and DC-STAMP, MetaMorph Software was used to calculate the area that had been selected above the threshold in 3 pixels of colocalized signals. The lipid rafts were labeled with a Vybrant AlexaFluor-488 Lipid Raft Labeling Kit (Thermo Fisher Scientific).

Planar lipid bilayer workstation

A lipid mixture of POPE (1-palmitoyl-2-oleoyl-*sn*-glycero-3-phosphoethanolamine) and DOPC (1,2-dioleoyl-*sn*-glycero-3-

membrane pattern of colocalized mStom and DC-STAMP (*c*, *d*), but control showed a homogeneous distribution (insets *a* and *b*). The average colocalized area of mStom and DC-STAMP was represented per capture field and examined by MetaMorph Software; cell–cell contact sites with abundant colocalized signals are shown (arrowheads) ($n = 3$ independent experiments). Scale bar, 50 μm. *C*) Western blot showing decreased stomatin protein expression by STOM-KD1 and -KD2. Densitometry values for mStom were normalized to the β-tubulin level ($n = 5$ independent experiments). RANKL stimulation increased DC-STAMP expression in $RAW^{Luc\text{-}KD}$ control cells; the increase was inhibited by knockdown of stomatin ($n = 3$ independent experiments). *D*, *E*) TRAP assays were performed in knockdown cells. RANKL-induction rendered most RAW cells $TRAP^+$. In contrast, the formation of MNCs (arrowheads) was greatly inhibited by stomatin-knockdown, especially by STOM-KD2. Scale bars, 1 mm (top and middle) and 100 μm (bottom). Each experiment contained 3 technical replicates; their average was calculated as 1 data point for that specific experiments ($n = 4$ independent experiments). All data are means ± SD. $^*P < 0.05$, by paired Student's *t* test.

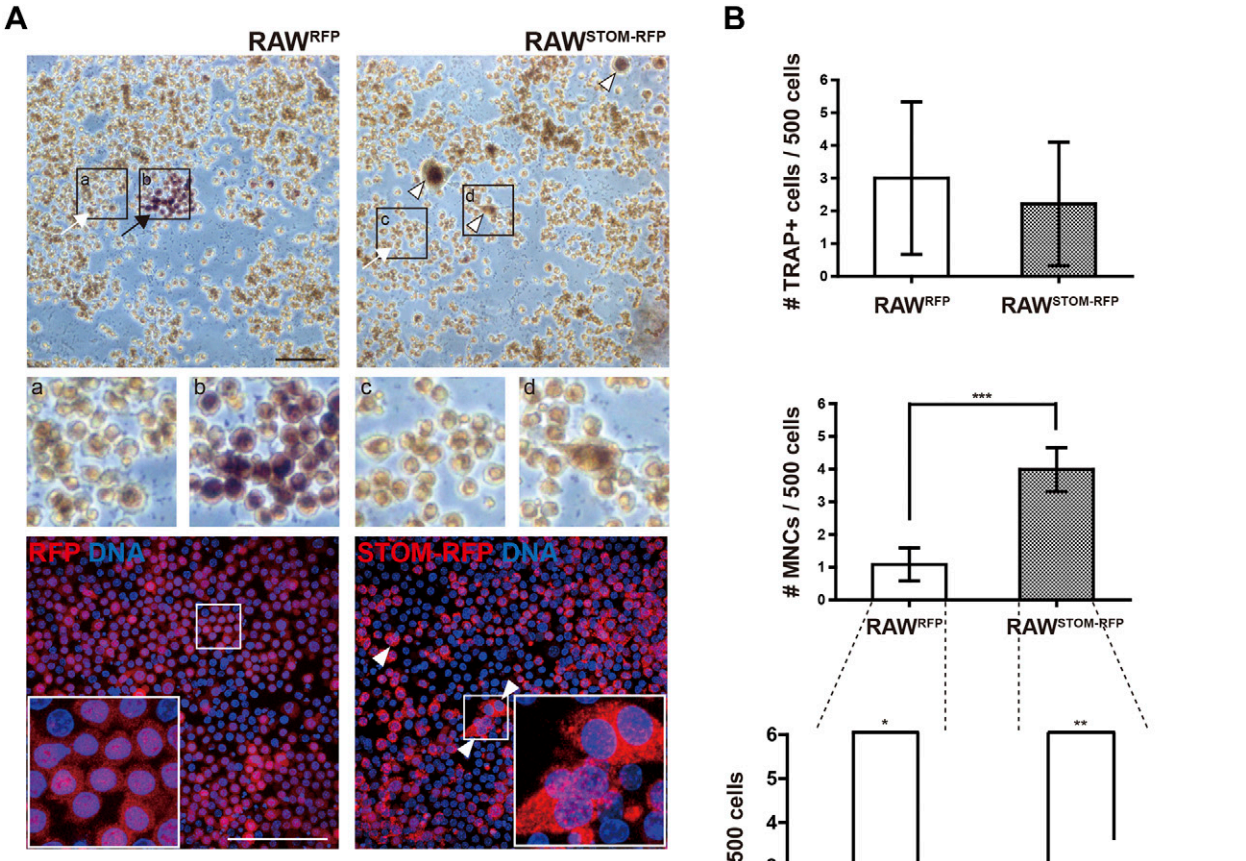

C

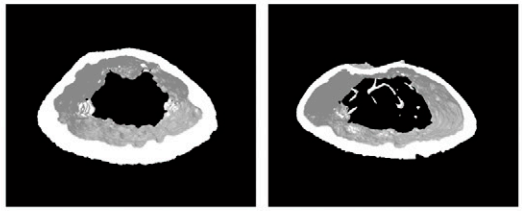

	WT (N=11)	STOM-Tg (N=11)	P value
% Porosity	13.62±0.76	14.58±1.21	0.0309

D

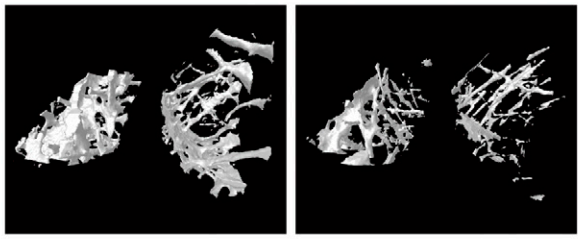

	WT (N=11)	STOM-Tg (N=11)	P value
BV / TV	6.82±2.40	4.05±2.20	0.0076
Tb. Th. (mm)	0.07±0.01	0.06±0.00	0.0111
Tb. No. (1/mm)	1.05±0.29	0.68±0.37	0.0093
Tb. Sp. (mm)	0.34±0.05	0.46±0.18	0.0327

Figure 4. Stomatin promotes bone resorption. *A*, *B*) RAW cells were transduced by lentivirus to express STOM-RFP or RFP; $RAW^{STOM\text{-}RFP}$ or RAW^{RFP} cells were subjected to TRAP and DNA staining. Most $RAW^{STOM\text{-}RFP}$ and RAW^{RFP} cells were $TRAP^{-}$ (white arrows; *a*, *c*). Only very few clusters of $TRAP^{+}$ cells (black arrow; *b*) were found in the RAW^{RFP} plate, and even less in the $RAW^{STOM\text{-}RFP}$ plate. Formation of MNCs was significantly increased by up-regulating stomatin expression. Without RANKL stimulation, <0.2% of RAW^{RFP} cells were MNCs, but the number increased 4-fold in $RAW^{STOM\text{-}RFP}$ cells (arrowheads; *d*). Most MNCs remained $TRAP^{-}$ (n = 3 independent experiments, each 3 technical replicates). Scale bar, 100 μm. *C*, *D*) Cortical and

(*continued on next page*)

phosphocholine) (1:4 weight ratio, 5 mg/ml) dissolved in *n*-hexane at 1 mg/ml was painted onto the aperture in a Delrin cup (diameter of aperture, 150 μm) and dried under N_2. In consecutive steps, 5 μl stock solutions of recombinant proteins (GST and GST-STOM; 0.5 μg/μl) were added to the Delrin cup and dried under N_2. The Delrin cup was then inserted into the cup holder, and both reservoirs were filled with 1 ml of buffer (300 mM KCl, 5 mM HEPES; pH 7.2). Then the lipid/protein mixture was painted with a brush across the aperture under a constant voltage of 80 mV, to support membrane association (36). Experimental data were recorded at room temperature with a planar lipid bilayer workstation (Warner Instruments, Hamden, CT, USA), with a BC-353 amplifier and 1440A data-acquisition system. Records were recorded at 5 kHz and filtered at 10 Hz with a Bessel 8-pole low-pass filter.

STOM-Tg mouse generation and μ-CT analysis

h*STOM* was cloned into vector STO-p1033 [modified and kindly provided by Dr. Ting-Fen Tsai, Institute of Genome Sciences, National Yang-Ming University) (37)] to drive stomatin gene expression by the RNA polymerase II large subunit promoter. Stomatin transgenic (STOM-Tg) mice were generated by pronuclear microinjection into C57BL/6 fertilized eggs. Tail DNA was used to examine genotype of mice by PCR. To analyze the murine physiology, a microcomputed tomography (μ-CT) scanner (SkyScan 1076; Bruker, Kontich, Belgium) was used at the Taiwan Mouse Clinic (Academia Sinica), to acquire data and 3-dimensional (3D) images from cortical and spongy bone of femurs of 76-wk-old male WT ($n = 3$) and STOM-Tg ($n = 3$) mice and 12- or 34-wk-old female WT ($n = 8$) and STOM-Tg ($n = 8$) mice. For cortical bone porosity or trabecular bone analysis and 3D images, a μ-CT scanner was operated at 50 kV, 140 μA, 0.8° rotation steps, 0.5 mm Al filter, and 9 μm image pixel size of scan resolution. Cross-sections were reconstructed with a cone-beam algorithm (NRecon software; Bruker). File data sets were then imported into CTAn software (Bruker) with a region of interest of 1.5 mm that was 0.4 mm away from the growth plate level in the direction of the metaphysis, to calculate 3D analysis and image generation.

BMDC preparation and osteoclastogenesis

The BMDCs were acquired from femurs of the C57BL/6 WT or STOM-Tg mice. RPMI1640 medium (HyClone) containing 10% FBS, 1% penicillin-streptomycin liquid (HyClone), and 30 ng/ml macrophage–colony stimulating factor (M-CSF; PeproTech, Rocky Hill, NJ, USA) was used to culture 1.0×10^7 BMDCs per 100-mm dish for 3 d. After 3 d of culture, 5.0×10^5 BMDCs were seeded onto 35-mm dishes with 200 ng/ml RANKL (PeproTech) plus 30 ng/ml M-CSF for 9 d, and refed with fresh medium every 3 d. Osteoclastogenesis was also induced in the cell line RAW264.7 (5.0×10^4 cells were seeded onto 35-mm culture dishes), with 50 ng/ml RANKL for 7 d and refed with fresh medium every 3 d. The cell samples were analyzed for osteoclastogenesis with the tartrate-resistant acid phosphatase (TRAP) assay (Sigma-Aldrich). A color CCD camera (CoolSNAP, Tucson, AZ, USA) on an inverted microscope (DM-IRBE; Leica) with a ×10 0.25 NA N Plan objective lens (Leica) was used to capture $TRAP^+$ cells, and we randomly chose areas of interest for quantification only from the central region of the culture plates to avoid potential bias resulting from different cell densities. The number of MNCs per 500 cells was counted under high magnification.

RESULTS

Increased expression of stomatin causes MNC formation resulting from cell–cell fusion

The human stomatin gene (*STOM*) tagged with GFP or the *GFP* gene alone was engineered and transfected into CHO K1 cells, generating $CHO^{STOM\text{-}GFP}$ and CHO^{GFP} cells, respectively. After 3 d of culture, we noted that the number of MNCs (**Fig. 1*A***) was significantly increased in $CHO^{STOM\text{-}GFP}$ cells that expressed a high level of stomatin compared with control CHO^{GFP} cells. Some MNCs contained 2 nuclei per cell, whereas others had 3 or more nuclei (Fig. 1*A*; quantified in Fig. 1*B*). Furthermore, MNC formation increased over time (Supplemental Fig. 1*A*), typically reaching a 3-fold increase compared to the control group in 3 d. A high content of stomatin induced MNC formation, not only in CHO cells but also in human embryonic kidney (HEK) 293T cells (Supplemental Table 1). Time-lapse images were obtained to record the process of MNC formation. In one series of events exemplified in Fig. 1*C*, in a cell undergoing cell division (1:00:00–1:48:00) mitosis was noted to stop (1:48:00 ~ 3:00:00), and the cell then went through cytokinesis failure or refusion (38) (3:00:00–3:54:00) to form a double-nuclear cell. In another series of events exemplified in Fig. 1*D*, 2 adjacent cells were noted to come into contact and then to undergo cell fusion (1:18:00–2:24:00). To distinguish MNCs formed by refusion from cell fusion, cells stably expressing GFP- or RFP-tagged stomatin ($CHO^{STOM\text{-}GFP}$ or $CHO^{STOM\text{-}RFP}$) were cocultured for 3 d. MNCs formed by refusion should contain only green or red fluorescence, whereas MNCs resulting from cell fusion should contain both fluorescences that could be identified and quantified by confocal microscopy (Fig. 1*E*) or flow cytometry (Supplemental Fig. 1*B*). Results from these experiments revealed that at least half of the MNCs induced by high levels of stomatin were formed *via* cell fusion. Cells of different animal species (CHO and HEK-293T cells; Supplemental Fig. 1*C*) fused with one another in the presence of highly abundant stomatin.

Exogenous stomatin also induces cell–cell fusion

It is generally thought that stomatin associates with the inner leaflet of the lipid bilayer *via* palmitoylation modification and hydrophobic domain (28, 29). Given such molecular characteristics, it is interesting to note that stomatin produced in the cells can be detected in the extracellular environment. The release and accumulation of extracellular stomatin in $CM\text{-}_{pro}CHO^{STOM\text{-}GFP}$ increased over time (**Fig.**

spongy bone of femurs from STOM-Tg mice ($n = 11$) were analyzed by μ-CT and compared to femurs of WT mice ($n = 11$). BV/TV indicates bone volume density. Tb Th, trabecular thickness; Tb No, trabecular number; Tb Sp, trabecular separation. Data are means ± SD. $*P < 0.05$, $**P < 0.01$, $***P < 0.001$, by paired Student's *t* test.

2*A*). In contrast, little GFP protein was detected in CM-$_{pro}$CHO^{GFP}. Western blot analysis revealed that hSTOMs were found, not only in the lysates from cells producing stomatin ($_{pro}$CHO^{STOM}), but also in the extracellular culture medium (or CM, CM-$_{pro}$CHO^{STOM}) and exosomes (Exosome--$_{pro}$CHO^{STOM}) (Fig. 2*B*). Although the mechanism for stomatin secretion is not clear, we speculate that stomatin found in the CM was not related to lysis of cells, because tubulin was not detected. We then examined whether the extracellular stomatin was functional. To do so, $_{pro}$CHO^{STOM} or $_{pro}$CHO (control) cells were plated on the top insert of a Transwell cell-migration culture chamber (Fig. 2*C*). We found that stomatin proteins released by $_{pro}$CHO^{STOM} cells diffused across the permeable membrane to reach the bottom chamber, where extracellular stomatin could bind to or be internalized by $_{rec}$CHO cells seeded in the bottom chamber, as evidenced by immunofluorescence and Western blot assay (Fig. 2*C*). In another series of experiments, purified recombinant stomatin produced by *Escherichia coli* or filtered CM-$_{pro}$CHO^{STOM} was applied to CHO cells for functional testing. After 3 d, both treatments effectively produced MNCs (Supplemental Table 1) formed *via* cell fusion (Fig. 2*D*). These results support the notion that stomatin proteins can be released by the cells selectively expressing the stomatin gene, and the extracellular stomatin can affect cells in their surroundings.

Stomatin affects MNC formation but not TRAP expression during RANKL-mediated osteoclastogenesis

Treating murine RAW cells with RANKL induced TRAP expression and MNC formation, given that these macrophage/monocyte cells progressively differentiated into OCs (2, 39). We speculated whether stomatin was involved in such processes. To address this question, we performed Western blot analysis to determine murine stomatin (mStom) and DC-STAMP expression during RANKL treatment (**Fig. 3*A***). Stimulating RAW cells with RANKL up-regulated the expression of DC-STAMP, a membrane protein essential for cell fusion during osteoclastogenesis (2, 40), and of mStom. Much more abundant mStom was found on the released exosomes from RANKL-treated RAW cells. In addition, immunofluorescence analysis of mStom and DC-STAMP distribution after RANKL treatment indicated obvious colocalization of mStom with DC-STAMP in cell–cell contact sites (Fig. 3*B*), more extensive in RANKL-treated RAW cells compared to the control, and part of the stomatin was on the lipid rafts (Supplemental Fig. 2). Moreover, 2 shRNAs (STOM-KD1 and -KD2) against different target sites of stomatin were individually introduced through lentiviral particles into RAW cells (RAW$^{STOM\text{-}KD1}$ and RAW$^{STOM\text{-}KD2}$). Both constructs effectively down-regulated stomatin expression in RAW cells, with STOM-KD2 (~80%) appearing to be more potent than STOM-KD1 (~70%) (Fig 3C). Such a RANKL-mediated DC-STAMP increase was profoundly inhibited in RAW$^{STOM\text{-}KD1}$ or RAW$^{STOM\text{-}KD2}$ cells by stomatin knockdown, compared to the control RAW$^{Luc\text{-}KD}$ cells. In the control, RANKL treatments also caused RAW cells to form MNCs (Fig. 3*D*); thus, RANKL-induced cell fusion was inhibited by stomatin knockdown treatments, with STOM-KD2 appearing to be more potent than STOM-KD1 (Fig. 3*D*; quantified in Fig. 3*E*). Production of TRAP after RANKL treatment was not inhibited by stomatin down-regulation (Fig. 3*D*). Although RAW$^{STOM\text{-}KD1}$ or RAW$^{STOM\text{-}KD2}$ cells remained mononuclear after RANKL stimulation, most if not all of them became TRAP$^+$.

In contrast, transduction of stomatin into RAW$^{STOM\text{-}RFP}$ cells caused them to undergo cell fusion, forming MNCs in the absence of RANKL (**Fig. 4*A***; quantified in Fig. 4*B*); however, most of the resulting MNCs remained TRAP$^-$. The control RAW^{RFP} cells were mostly mononuclear and TRAP$^-$ (Fig. 4*A*), without RANKL stimulation. Occasionally, there were clusters of TRAP$^+$ cells found in both control RAW^{RFP} and RAW$^{STOM\text{-}RFP}$ cells (Fig. 4*B*); the occurrences of TRAP$^+$ cells were probably caused by trimerization of RANK receptor (41). Such findings indicate that stomatin is crucial for MNC formation in osteoclastogenesis; nevertheless, TRAP activity may not be related to the stomatin expression level.

Increased stomatin expression induces an osteoporosis phenotype in mice

STOM-Tg mice were generated to reveal the role of stomatin in animals. Analysis by μ-CT showed that porosity of cortical bone was significantly higher in STOM-Tg mice than in WT mice (Fig. 4*C* and **Table 1**). In addition, examination of the spongy bone in the femur according to various parameters, such as bone volume (bone volume/total volume; BV/TV), trabecular bone (Tb) thickness (Th), Tb number (No), and Tb separation (Sp), demonstrated an osteoporosis phenotype in STOM-Tg mice, compared to the WT (Fig. 4*D* and Table 1). BMDCs from WT and STOM-Tg mice were also obtained and subjected to RANKL stimulation. We found that the basal level of DC-STAMP and RANKL-induced DC-STAMP increase were both higher in STOM-Tg BMDCs than in WT BMDCs (Supplemental Fig. 3*A*). Microscopic examination after a TRAP staining assay demonstrated that STOM-Tg BMDCs gave rise to more TRAP$^+$ MNCs (or OCs) after RANKL treatment than WT BMDCs (Supplemental Fig. 3*B*). These results support the notion that high-level expression of stomatin in STOM-Tg mice promotes differentiation and cell fusion of OCs, resulting in enhanced bone resorption and an osteoporosis phenotype.

TABLE 1. *Comparison of femurs in WT and STOM-Tg mice*

Characteristic	WT (n = 11)	STOM-Tg (n = 11)	P
Cortical porosity(%)	13.62 ± 0.76	14.58 ± 1.21	0.0309
Spongy bone			
BV/TV	6.82 ± 2.40	4.05 ± 2.20	0.0076
Tb Th (mm)	0.07 ± 0.01	0.06 ± 0.00	0.0111
Tb No (1/mm)	1.05 ± 0.29	0.67 ± 0.37	0.0093
Tb Sp (mm)	0.34 ± 0.05	0.46 ± 0.18	0.0327

Stomatin disturbs membrane integrity

Next, to explore the effect of stomatin on the membrane, the recombinant protein stomatin was expressed in *E. coli*, purified, and reconstituted into lipid membranes. Under constant-voltage conditions, stomatin rendered the membrane permeable to ions (**Fig. 5*A***). Several conductance levels in the range of 50–90 pS were detected. The events lasted over several seconds. Occasionally, protein assemblies appeared to switch between the 2 levels, directly and dynamically. As a control, GST from vector did not exhibit any membrane activity (Fig. 5*B*). These results indicate that stomatin, by forming dynamic assemblies, can disturb the membrane and enable ion flux across it.

DISCUSSION

A schematic model illustrating proposed roles of stomatin for cell fusion during osteoclastogenesis is shown in **Fig. 6**. Stomatin is an integral membrane protein (21) that is widely expressed in many cell types and is associated with lipid rafts (23, 24, 42). It is generally accepted that stomatin has a unique hairpin-loop topology (32, 43). It contains a hydrophobic domain toward its N terminus (43). This motif, together with several palmitoylation sites flanking the hydrophobic domain (28, 29), helps anchor the molecule to the inner leaflet of the lipid bilayer. Both the N and C termini of stomatin face the cytoplasm (32, 33). In such a scenario, stomatin synthesized in the cytoplasm can be translocated either by diffusion (Fig. 6, *1*) or through vesicular transport (Fig. 6, *1′*) to the plasma membrane with a predicted signaling peptide sequence (44). The membrane-associated stomatin proteins are present in high abundance within lipid rafts, the sphingolipid- and cholesterol-rich membrane microdomains that preferentially contain lipid-modified proteins (21). In addition to the hairpin-loop topology, stomatin may exist as a single-pass transmembrane structure with intracellular N terminus and extracellular C terminus (33). In this topology, transmembranous stomatin proteins can also translocate to the plasma membrane *via* a conventional secretory pathway (Fig. 6, *1′*). Experimental evidence supports the notion that both topologies coexist through differential folding of stomatin.

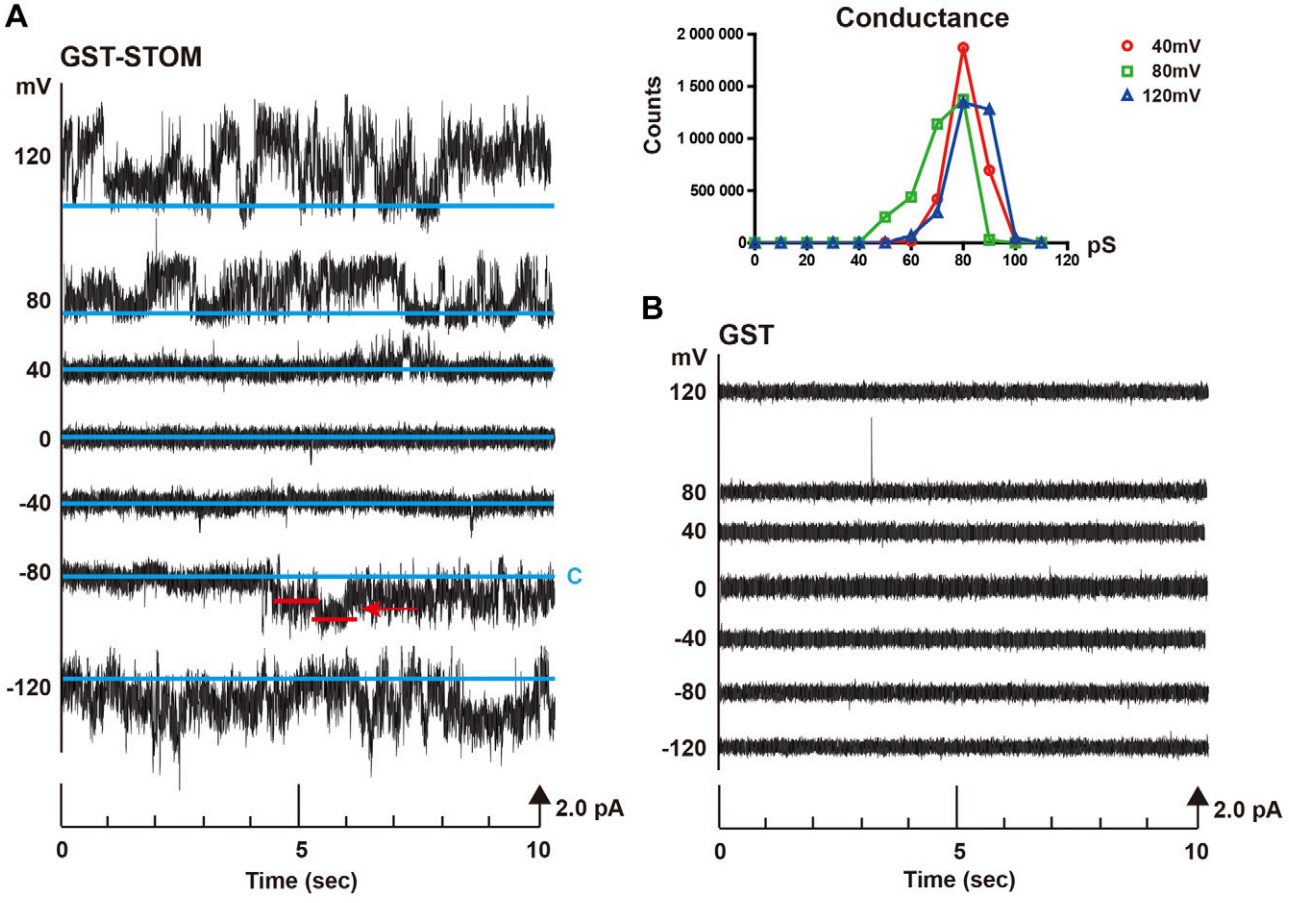

Figure 5. Stomatin interrupts membrane integrity. After reconstituting recombinant GST-stomatin proteins (*A*) and control GST (*B*) into a planar lipid bilayer of a 1:4 mixture of POPE and DOPC, dynamic changes in currents (pA) at various holding potentials (in millivolts) across the artificial membrane were recorded. For individual traces, deviations from the blue line (c, closed state) indicated increase of membrane permeability; conductance in Siemens could be calculated by amp/volt (top right). Recordings were conducted in a buffer solution of 300 mM KCl and 5 mM HEPES (pH 7.2). A typical example of 3 experiments is shown.

In this study, we found that intracellular stomatin can be released into the extracellular environment. It is unclear whether and how stomatin, in either the inner leaflet membrane-anchored proteins or single-pass transmembrane protein form, is released into the culture medium (Fig. 6, *2*; see Fig. 2*A*, *B*). Equally unclear is how the released free stomatin outside of a cell is internalized by another cell (Fig. 6, *3*; see Fig. 2*C*). A recent study of exosomes, a special category of extracellular vesicles (45), provides a possible mechanism for stomatin secretion and uptake. In biologic fluids, including cultured medium, the cell-derived exosomes are smaller than the pore size of a Transwell cell-migration membrane and cannot be excluded by filtering CM (Fig. 2*A*–*C*). We observed that extracellular stomatin was present in exosomes (Figs. 2*B* and 3*A*), which are released from the cell when multivesicular bodies (MVBs) containing stomatin fused with the plasma membrane (Fig. 6, *2′*) (22, 45). Extracellular exosomes carrying various proteins can fuse with target cell membranes, either directly with the plasma membrane or with the endosomal membrane after endocytosis. Exosomes can thus transfer molecules, such as stomatin, from one cell to another *via* membrane vesicle trafficking (Fig. 6, *3′*; see Fig. 2*C*). After entering the target cell, the cytoplasmically oriented integral membranous stomatin may form high-order oligomers within lipid rafts (Supplemental Fig. 2) and execute its functions (Fig. 6, *4*) (30, 31). The plasma membrane is highly mosaic, with different lipid and protein levels in the dynamics and the clusters of variable sizes; the lipid rafts represent one such example. Within the lipid rafts, the spatial and temporal heterogeneity can be further modulated by the interplay among lipids and proteins. We hypothesize that stomatin oligomers, by restricting lateral diffusion or "corralling" membrane proteins within the lipid rafts, affect the intermolecular actions of membrane receptors and their ligands or effectors, to regulate downstream signal transduction (Fig. 6, *4*).

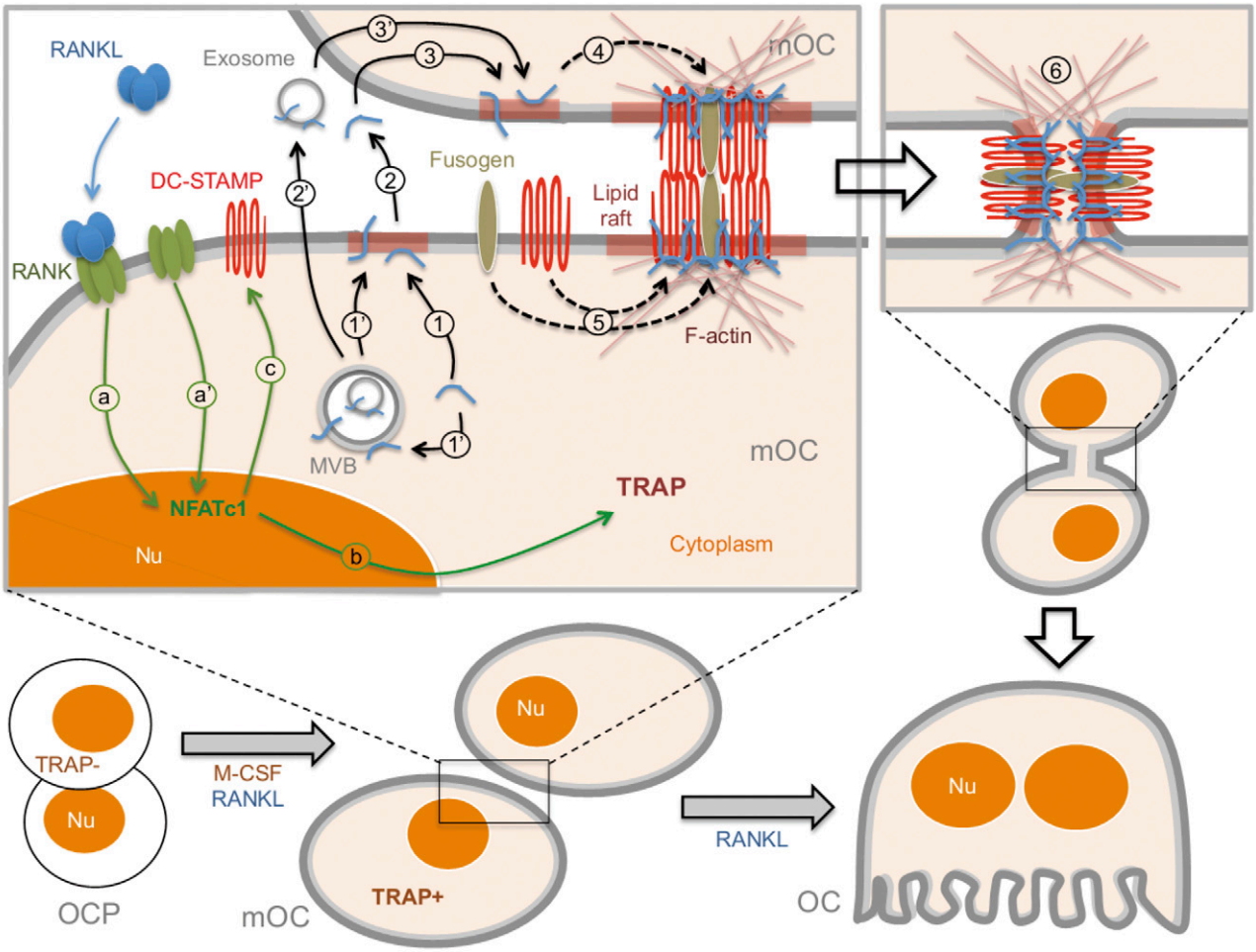

Figure 6. Schematic model illustrating proposed roles of stomatin for cell fusion during osteoclastogenesis. A schematic model illustrating a hypothetic model for the release of stomatin and uptake through membrane anchor (1→2→3), extracellular vesicle, or exosome pathway (1′→2′→3′) and its corralling role in the lipid raft membrane microdomains (*4*) that enhances intermolecular interactions between fusogenic DC-STAMP and other putative fusogens (*5*). In this scenario, stomatin can potentiate cell fusion activity triggered by RANKL stimulation (*a*) during osteoclastogenesis, without affecting TRAP expression (*b*). See text for details. Nu, nucleus; OCP, osteoclast progenitor; mOC, mononuclear osteoclast; OC, multinuclear osteoclast. MVB, multivesicular body; lipid rafts, membrane labeled red.

The role of stomatin in cell fusion was tested by an osteoclastogenesis model. Treating OC progenitor (OCP) cells with M-CSF/RANKL turned mononuclear $TRAP^-$ OCPs into $TRAP^+$ mononuclear (m)OCs. Further RANKL treatment of mOCs triggered cell fusion, forming multinuclear $TRAP^+$ mature OCs. As shown in Fig. 6, binding of RANKL to RANK receptors on RAW cells (Fig. 6, *a*) activated NFATc1 transcription factor to turn on TRAP expression (*b*) and increased expression of DC-STAMP (*c*) (39, 40). Interactions of DC-STAMP and possibly other fusogenic molecules (fusogen in Fig. 6) residing on the plasma membrane trigger fusion at the site of intercellular contact. We hypothesize that such intermolecular interactions between cells are facilitated by stomatin oligomers that enhance membrane fusion complex formation within the lipid rafts (Fig. 6, *5*; see Fig. 3*B* and Supplemental Fig. 2), and the molecular complex forms a zippering or hairpin structure that bends membrane to induce fusion pore expansion, as a prelude to cell fusion (Fig. 6, *6*). Therefore, we propose that stomatin does not initiate cell fusion, but instead works as an "enhancer" to potentiate cell-fusion events. This notion is supported by the finding that a decrease in stomatin hindered DC-STAMP-mediated cell fusion but not TRAP expression in RANKL-stimulated RAW cells, resulting in formation of $TRAP^+$ mononuclear cells (Fig. 3*D*). In contrast, an increase in stomatin causes RAW cells to fuse, even in the absence of RANKL stimulation, resulting in the formation of $TRAP^-$ MNCs (Fig. 4*A*). Occasionally, physiologic-level RANK receptors on RAW cells can spontaneously trimerize to trigger low-level signaling and induce TRAP synthesis but not cell fusion (Fig. 6*a*′) (41), resulting in formation of $TRAP^+$ mononuclear cells (see Fig. 4*A*, *b*).

In terms of molecular property, stomatin may not serve as the receptor that initiates the cell fusion process for small proteins (31.5 kDa). It is also not likely that stomatin can function as an effector that mediates hemifusion and fusion pore formation. Our data support the notion that high content of stomatin increases effectiveness of molecular machinery for cell fusion by recruiting existing fusogenic receptor/effectors to the (lipid rafts) sites of cell–cell contact and enhance their interactions. The unique protein refolding property of stomatin between the hairpin and single-pass transmembrane topology offers 2 implications: on the one hand, stomatin, through the corralling effect, can facilitate interactions among fusogenic proteins, either within the membrane microdomain or across the appositional membranes. On the other hand, it may help relieve the membrane curvature stress by increasing permeability (Fig. 5*A*) (35) and cause clustering of the fusogenic molecular assembly to the cortical actin cytoskeleton, as either a rigid supportive platform (Fig. 6, *6*) or a tethered site for actin polymerization that generates force to drive expansion of fusion pores.

We have shown in STOM-Tg mice that, through overactive osteoclastogenesis, a high level of stomatin leads to an osteoporosis phenotype (Fig. 4*C*, *D*). Differentiation and maturation of OCs are characterized by both MNC formation and synthesis of bone-resorbing enzymes. The finding that stomatin regulates cell fusion without interfering with enzyme production may provide new opportunities for correcting bone loss disorders by inhibiting the molecular events associated with membrane fusion. FJ

ACKNOWLEDGMENTS

The authors thank Dr. Li-Li Li (Institute of Microbiology and Immunology, National Yang-Ming University) for her helpful proof-reading of the manuscript; Dr. Chien-Yi Tung (Institute of Microbiology and Immunology, National Yang-Ming University) for the statistical analysis; Chia-Wen Wang (Institute of Biophotonics, National Yang-Ming University) for the operation of planar lipid bilayer system; the Molecular and Genetic Imaging Core from the National Research Program for Genomic Medicine (NRPGM); and the Taiwan Mouse Clinic (TMC) from the National Research Program for Biopharmaceutics (NRPB) Resource Center for technical support. This work was supported by the Ministry of Education, Aim for the Top University Plan: MOST 104-2319-B-010-001. The authors declare no conflicts of interest.

AUTHOR CONTRIBUTIONS

J.-H. Lee, C- F. Hsieh, and C.-H. Lin designed the research; J.-H. Lee performed the research and analyzed the data; H.-W. Liu and T.-W. Chen contributed microscopic approaches; C.-Y. Chen, S.-C. Wu, C.-S. Hsu, Y.-H. Liao, and C.-Y. Yang contributed materials; J.-F. Shyu and W. B. Fischer helped with the osteoclast culture and lipid-bilayer system, respectively; and J.- H. Lee, H.-W. Liu, and C.- H. Lin wrote the manuscript.

REFERENCES

1. Wooding, F. B. (1992) Current topic: the synepitheliochorial placenta of ruminants: binucleate cell fusions and hormone production. *Placenta* **13**, 101–113
2. Yagi, M., Miyamoto, T., Sawatani, Y., Iwamoto, K., Hosogane, N., Fujita, N., Morita, K., Ninomiya, K., Suzuki, T., Miyamoto, K., Oike, Y., Takeya, M., Toyama, Y., and Suda, T. (2005) DC-STAMP is essential for cell-cell fusion in osteoclasts and foreign body giant cells. *J. Exp. Med.* **202**, 345–351
3. Millay, D. P., O'Rourke, J. R., Sutherland, L. B., Bezprozvannaya, S., Shelton, J. M., Bassel-Duby, R., and Olson, E. N. (2013) Myomaker is a membrane activator of myoblast fusion and muscle formation. *Nature* **499**, 301–305
4. Podbilewicz, B., Leikina, E., Sapir, A., Valansi, C., Suissa, M., Shemer, G., and Chernomordik, L. V. (2006) The C. elegans developmental fusogen EFF-1 mediates homotypic fusion in heterologous cells and in vivo. *Dev. Cell* **11**, 471–481
5. Fujiwara, T., Bandi, M., Nitta, M., Ivanova, E. V., Bronson, R. T., and Pellman, D. (2005) Cytokinesis failure generating tetraploids promotes tumorigenesis in p53-null cells. *Nature* **437**, 1043–1047
6. Hu, C., Ahmed, M., Melia, T. J., Söllner, T. H., Mayer, T., and Rothman, J. E. (2003) Fusion of cells by flipped SNAREs. *Science* **300**, 1745–1749
7. Novick, P., Field, C., and Schekman, R. (1980) Identification of 23 complementation groups required for post-translational events in the yeast secretory pathway. *Cell* **21**, 205–215
8. Balch, W. E., Dunphy, W. G., Braell, W. A., and Rothman, J. E. (1984) Reconstitution of the transport of protein between successive compartments of the Golgi measured by the coupled incorporation of N-acetylglucosamine. *Cell* **39**, 405–416
9. Hanson, P. I., Roth, R., Morisaki, H., Jahn, R., and Heuser, J. E. (1997) Structure and conformational changes in NSF and its membrane receptor complexes visualized by quick-freeze/deep-etch electron microscopy. *Cell* **90**, 523–535
10. Bullough, P. A., Hughson, F. M., Skehel, J. J., and Wiley, D. C. (1994) Structure of influenza haemagglutinin at the pH of membrane fusion. *Nature* **371**, 37–43
11. Mi, S., Lee, X., Li, X., Veldman, G. M., Finnerty, H., Racie, L., LaVallie, E., Tang, X.-Y., Edouard, P., Howes, S., Keith, J. C., Jr., and McCoy, J. M. (2000) Syncytin is a captive retroviral envelope protein involved in human placental morphogenesis. *Nature* **403**, 785–789

12. Chamberlain, L. H., Burgoyne, R. D., and Gould, G. W. (2001) SNARE proteins are highly enriched in lipid rafts in PC12 cells: implications for the spatial control of exocytosis. *Proc. Natl. Acad. Sci. USA* **98**, 5619–5624
13. Takeda, M., Leser, G. P., Russell, C. J., and Lamb, R. A. (2003) Influenza virus hemagglutinin concentrates in lipid raft microdomains for efficient viral fusion. *Proc. Natl. Acad. Sci. USA* **100**, 14610–14617
14. Ishii, M., Iwai, K., Koike, M., Ohshima, S., Kudo-Tanaka, E., Ishii, T., Mima, T., Katada, Y., Miyatake, K., Uchiyama, Y., and Saeki, Y. (2006) RANKL-induced expression of tetraspanin CD9 in lipid raft membrane microdomain is essential for cell fusion during osteoclastogenesis. *J. Bone Miner. Res.* **21**, 965–976
15. Tavano, R., Contento, R. L., Baranda, S. J., Soligo, M., Tuosto, L., Manes, S., and Viola, A. (2006) CD28 interaction with filamin-A controls lipid raft accumulation at the T-cell immunological synapse. *Nat. Cell Biol.* **8**, 1270–1276
16. Li, N., Mak, A., Richards, D. P., Naber, C., Keller, B. O., Li, L., and Shaw, A. R. (2003) Monocyte lipid rafts contain proteins implicated in vesicular trafficking and phagosome formation. *Proteomics* **3**, 536–548
17. Harder, T., Scheiffele, P., Verkade, P., and Simons, K. (1998) Lipid domain structure of the plasma membrane revealed by patching of membrane components. *J. Cell Biol.* **141**, 929–942
18. Viola, A., Schroeder, S., Sakakibara, Y., and Lanzavecchia, A. (1999) T lymphocyte costimulation mediated by reorganization of membrane microdomains. *Science* **283**, 680–682
19. Biswas, S., Yin, S. R., Blank, P. S., and Zimmerberg, J. (2008) Cholesterol promotes hemifusion and pore widening in membrane fusion induced by influenza hemagglutinin. *J. Gen. Physiol.* **131**, 503–513
20. Hess, S. T., Kumar, M., Verma, A., Farrington, J., Kenworthy, A., and Zimmerberg, J. (2005) Quantitative electron microscopy and fluorescence spectroscopy of the membrane distribution of influenza hemagglutinin. *J. Cell Biol.* **169**, 965–976
21. Salzer, U., and Prohaska, R. (2001) Stomatin, flotillin-1, and flotillin-2 are major integral proteins of erythrocyte lipid rafts. *Blood* **97**, 1141–1143
22. Salzer, U., Zhu, R., Luten, M., Isobe, H., Pastushenko, V., Perkmann, T., Hinterdorfer, P., and Bosman, G. J. (2008) Vesicles generated during storage of red cells are rich in the lipid raft marker stomatin. *Transfusion* **48**, 451–462
23. Feuk-Lagerstedt, E., Samuelsson, M., Mosgoeller, W., Movitz, C., Rosqvist, A., Bergström, J., Larsson, T., Steiner, M., Prohaska, R., and Karlsson, A. (2002) The presence of stomatin in detergent-insoluble domains of neutrophil granule membranes. *J. Leukoc. Biol.* **72**, 970–977
24. Mairhofer, M., Steiner, M., Mosgoeller, W., Prohaska, R., and Salzer, U. (2002) Stomatin is a major lipid-raft component of platelet alpha granules. *Blood* **100**, 897–904
25. Lande, W. M., Thiemann, P. V., and Mentzer, W. C., Jr. (1982) Missing band 7 membrane protein in two patients with high Na, low K erythrocytes. *J. Clin. Invest.* **70**, 1273–1280
26. Fricke, B., Argent, A. C., Chetty, M. C., Pizzey, A. R., Turner, E. J., Ho, M. M., Iolascon, A., von Düring, M., and Stewart, G. W. (2003) The "stomatin" gene and protein in overhydrated hereditary stomatocytosis. *Blood* **102**, 2268–2277
27. Zhu, Y., Paszty, C., Turetsky, T., Tsai, S., Kuypers, F. A., Lee, G., Cooper, P., Gallagher, P. G., Stevens, M. E., Rubin, E., Mohandas, N., and Mentzer, W. C. (1999) Stomatocytosis is absent in "stomatin"-deficient murine red blood cells. *Blood* **93**, 2404–2410
28. Umlauf, E., Mairhofer, M., and Prohaska, R. (2006) Characterization of the stomatin domain involved in homo-oligomerization and lipid raft association. *J. Biol. Chem.* **281**, 23349–23356
29. Snyers, L., Umlauf, E., and Prohaska, R. (1999) Cysteine 29 is the major palmitoylation site on stomatin. *FEBS Lett.* **449**, 101–104
30. Snyers, L., Umlauf, E., and Prohaska, R. (1998) Oligomeric nature of the integral membrane protein stomatin. *J. Biol. Chem.* **273**, 17221–17226
31. Brand, J., Smith, E. S., Schwefel, D., Lapatsina, L., Poole, K., Omerbašić, D., Kozlenkov, A., Behlke, J., Lewin, G. R., and Daumke, O. (2012) A stomatin dimer modulates the activity of acid-sensing ion channels. *EMBO J.* **31**, 3635–3646
32. Desneves, J., Berman, A., Dynon, K., La Greca, N., Foley, M., and Tilley, L. (1996) Human erythrocyte band 7.2b is preferentially labeled by a photoreactive phospholipid. *Biochem. Biophys. Res. Commun.* **224**, 108–114
33. Kadurin, I., Huber, S., and Gründer, S. (2009) A single conserved proline residue determines the membrane topology of stomatin. *Biochem. J.* **418**, 587–594
34. Chen, A., Leikina, E., Melikov, K., Podbilewicz, B., Kozlov, M. M., and Chernomordik, L. V. (2008) Fusion-pore expansion during syncytium formation is restricted by an actin network. *J. Cell Sci.* **121**, 3619–3628
35. Lim H. W. G., Wortis, M., and Mukhopadhyay, R. (2002) Stomatocyte-discocyte-echinocyte sequence of the human red blood cell: evidence for the bilayer- couple hypothesis from membrane mechanics. *Proc. Natl. Acad. Sci. USA* **99**, 16766–16769
36. Mehnert, T., Routh, A., Judge, P. J., Lam, Y. H., Fischer, D., Watts, A., and Fischer, W. B. (2008) Biophysical characterization of Vpu from HIV-1 suggests a channel-pore dualism. *Proteins* **70**, 1488–1497
37. Wu, C. Y., Chen, Y. F., Wang, C. H., Kao, C. H., Zhuang, H. W., Chen, C. C., Chen, L. K., Kirby, R., Wei, Y. H., Tsai, S. F., and Tsai, T. F. (2012) A persistent level of Cisd2 extends healthy lifespan and delays aging in mice. *Hum. Mol. Genet.* **21**, 3956–3968
38. Rengstl, B., Newrzela, S., Heinrich, T., Weiser, C., Thalheimer, F. B., Schmid, F., Warner, K., Hartmann, S., Schroeder, T., Küppers, R., Rieger, M. A., and Hansmann, M. L. (2013) Incomplete cytokinesis and re-fusion of small mononucleated Hodgkin cells lead to giant multinucleated Reed-Sternberg cells. *Proc. Natl. Acad. Sci. USA* **110**, 20729–20734
39. Takayanagi, H., Kim, S., Koga, T., Nishina, H., Isshiki, M., Yoshida, H., Saiura, A., Isobe, M., Yokochi, T., Inoue, J., Wagner, E. F., Mak, T. W., Kodama, T., and Taniguchi, T. (2002) Induction and activation of the transcription factor NFATc1 (NFAT2) integrate RANKL signaling in terminal differentiation of osteoclasts. *Dev. Cell* **3**, 889–901
40. Kukita, T., Wada, N., Kukita, A., Kakimoto, T., Sandra, F., Toh, K., Nagata, K., Iijima, T., Horiuchi, M., Matsusaki, H., Hieshima, K., Yoshie, O., and Nomiyama, H. (2004) RANKL-induced DC-STAMP is essential for osteoclastogenesis. *J. Exp. Med.* **200**, 941–946
41. Kanazawa, K., and Kudo, A. (2005) Self-assembled RANK induces osteoclastogenesis ligand-independently. *J. Bone Miner. Res.* **20**, 2053–2060
42. Umlauf, E., Csaszar, E., Moertelmaier, M., Schuetz, G. J., Parton, R. G., and Prohaska, R. (2004) Association of stomatin with lipid bodies. *J. Biol. Chem.* **279**, 23699–23709
43. Yokoyama, H., Fujii, S., and Matsui, I. (2008) Crystal structure of a core domain of stomatin from Pyrococcus horikoshii Illustrates a novel trimeric and coiled-coil fold. *J. Mol. Biol.* **376**, 868–878
44. Nielsen, H., Engelbrecht, J., Brunak, S., and von Heijne, G. (1997) Identification of prokaryotic and eukaryotic signal peptides and prediction of their cleavage sites. *Protein Eng.* **10**, 1–6
45. De Gassart, A., Geminard, C., Fevrier, B., Raposo, G., and Vidal, M. (2003) Lipid raft-associated protein sorting in exosomes. *Blood* **102**, 4336–4344

Received for publication May 23, 2016.
Accepted for publication September 7, 2016.

Lipid raft–associated stomatin enhances cell fusion

Jui-Hao Lee, Chia-Fen Hsieh, Hong-Wen Liu, et al.

FASEB J published online September 23, 2016
Access the most recent version at doi:10.1096/fj.201600643R